Frequency and Voltage Tuning of Series–Series Compensated Wireless Power Transfer System to Sustain Rated Power Under Various Conditions

Yiming Zhang, *Member, IEEE*, Tianze Kan, *Student Member, IEEE*, Zhengchao Yan, *Student Member, IEEE*, and Chunting Chris Mi, *Fellow, IEEE*

***Abstract*— In a wireless power transfer (WPT) system, voltage tuning and frequency tuning are two major methods to control the output power. For the design of a WPT system at the rated power, it is crucial to understand the characteristics of a WPT system with a constant-power load (CPL) under voltage tuning and frequency tuning. The model of a series–series compensated WPT system with a CPL is established based on the Thevenin equivalent circuits. The conditions to achieve the maximum coil-to-coil efficiency for the two tuning methods are obtained. For frequency tuning, the tuning zone above the resonant frequency is selected because of its wide tuning range and zero-voltage switching. The maximum output power at different operating frequencies is derived, and the required inverter dc voltage and the tuning range for a target output power can be obtained accordingly. With a strong coupling, the maximum efficiency of frequency tuning can be as high as that of voltage tuning; while with a weak coupling, the efficiency of frequency tuning is much smaller than that of voltage tuning. The model with a CPL is helpful for the design and optimization of a WPT system with the rated power.**

***Index Terms*— Constant power, frequency tuning, modeling, voltage tuning, wireless charging, wireless power transfer (WPT).**

I. Introduction

WIRELESS power transfer (WPT) [1]–[3] is the emerging technology that supplies power from the source to the load wirelessly, eliminating the direct contact between them. Inductive power transfer, a WPT technology based on magnetic induction, has attracted enormous attention in the past few years and has been applied in commercial markets such as consumer electronics and electric vehicles. WPT standards, such as Qi standard from the wireless power consortium and J2954 from the Society of Automotive Engineers, have been proposed to further extend the application of the WPT technology.

In low-power and medium-power applications, either the ac output voltage or the operating frequency [4]–[9] of the inverter can be regulated for a target output, corresponding to voltage tuning and frequency tuning. In voltage tuning, either amplitude control [10] or phase shift control [11] can be utilized. They are equivalent in that the root-mean-square value of the inverter ac voltage is adjusted. Phase shift control is faster in response but may lose soft switching of the switches. Amplitude control is slower but can maintain soft switching status. Only amplitude control for voltage tuning is considered.

In the design of a WPT system with the rated output power, it is crucial to understand the characteristics of outputting this target power in different operating conditions. Selecting an operating point that satisfies certain conditions is of great importance to the design and optimization of a WPT system. For voltage tuning, selecting the inverter and rectifier dc voltages (U_{inv} and U_{rec}) to achieve the maximum efficiency at the target output power should be investigated. For frequency tuning, it remains unclear how to achieve the maximum efficiency, how to predict the maximum output power under different operating frequencies for a given U_{inv}, and how the coupling coefficient (k) affects the transfer characteristics. Therefore, it is crucial to build the mathematical model of a WPT system with a constant-power load (CPL) under voltage tuning and frequency tuning. In the current literature, the WPT system is usually modeled as either a constant-resistance load [12]–[15] or a constant-voltage load (CVL) [16]–[18]. These models are not adequate to analyze a WPT system with a CPL via voltage tuning or frequency tuning.

This paper analyzes the transfer characteristics of a series–series (SS) compensated WPT system with a CPL via voltage tuning and frequency tuning, respectively. The Thevenin equivalent circuits (TECs) of the WPT system reflected on the receiver side are developed. Voltage tuning is analyzed in Section II, followed by frequency tuning in Section III. The theoretical calculations and experimental results are conducted in Section IV to validate the analysis.

II. Voltage Tuning

Manuscript received January 11, 2018; revised March 16, 2018, July 13, 2018, and August 28, 2018; accepted September 18, 2018. Date of publication September 24, 2018; date of current version May 1, 2019. This work was supported in part by the Department of Energy, Argonne National Laboratory, U.S.-China Clean Energy Center under Grant DE-AC02-06CH11357, and in part by Huawei Technologies Co., Ltd., under Grant 9406139. Recommended for publication by Associate Editor Chi K. Lee. *(Corresponding author: Chunting Chris Mi.)*

Y. Zhang, T. Kan, and C. C. Mi are with the Department of Electrical and Computer Engineering, San Diego State University, San Diego, CA 92182 USA (e-mail: zhangym07@gmail.com; bigtreehust@gmail.com; mi@ieee.org).

Z. Yan is with the School of Marine Science and Technology, Northwestern Polytechnical University, Xi'an 710072, China, and also with the Department of Electrical and Computer Engineering, San Diego State University, San Diego, CA 92182 USA (e-mail: yanzc1991@gmail.com).

Color versions of one or more of the figures in this paper are available online at http://ieeexplore.ieee.org.

Digital Object Identifier 10.1109/JESTPE.2018.2871636

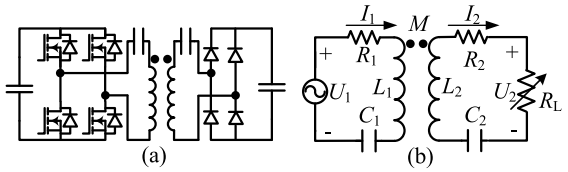

Fig. 1. SS compensated WPT system. (a) Topology. (b) Equivalent circuit.

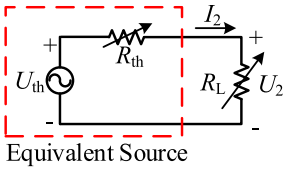

Fig. 2. TEC at resonance.

The topology and the equivalent circuit of a typical SS compensated WPT system are depicted in Fig. 1, where U_1 (U_2), I_1 (I_2), L_1 (L_2), C_1 (C_2), and R_1 (R_2) are the transmitter (receiver) voltage, current, inductance, capacitance, and equivalent resistance, respectively, M is the mutual inductance, and R_L is the equivalent load resistance.

Based on first harmonic approximation, we have $U_1 = 2\sqrt{2}/\pi \cdot U_{\text{inv}}$ and $U_2 = 2\sqrt{2}/\pi \cdot U_{\text{rec}}$. For voltage tuning of a WPT system, the operating angular frequency ω should equal the resonant angular frequency ω_0 to achieve the maximum coil-to-coil efficiency (η_{coil}) [19]. The resonant frequency f_0 should satisfy $f_0 = \omega_0/(2\pi) = 1/(2\pi\sqrt{L_1C_1}) = 1/(2\pi\sqrt{L_2C_2})$. The TEC with the parameters reflected on the receiver side is shown in Fig. 2.

U_{th} and R_{th} are the Thevenin voltage and resistance, respectively, and can be expressed by

$$U_{\text{th}} = \frac{\omega_0 M U_1}{R_1}, \quad R_{\text{th}} = R_2 + \frac{(\omega_0 M)^2}{R_1} \approx \frac{(\omega_0 M)^2}{R_1}. \tag{1}$$

A. Model With a CVL

For a given U_2, I_2, I_1, and the output power P_{out} can be derived as

$$I_2 = \frac{U_{\text{th}} - U_2}{R_{\text{th}}} \approx \frac{U_1}{\omega_0 M}, I_1 = \frac{U_2 + I_2 R_2}{\omega_0 M} \approx \frac{U_2}{\omega_0 M} \tag{2}$$

$$P_{\text{out}} = U_2 I_2 \approx \frac{U_1 U_2}{\omega_0 M}. \tag{3}$$

η_{coil} can thus be obtained as

$$\eta_{\text{coil}} = \frac{P_{\text{out}}}{P_{\text{out}} + I_1^2 R_1 + I_2^2 R_2} = \frac{\text{FOM}}{\text{FOM} + \frac{U_2}{U_1}\sqrt{\frac{R_1}{R_2}} + \frac{U_1}{U_2}\sqrt{\frac{R_2}{R_1}}}. \tag{4}$$

In (4), figure of merit (FOM) is defined as

$$\text{FOM} = \frac{\omega_0 M}{\sqrt{R_1 R_2}} = k\sqrt{\frac{\omega_0 L_1}{R_1}\frac{\omega_0 L_2}{R_2}} = k\sqrt{Q_1 Q_2} \tag{5}$$

where $Q_1 = \omega_0 L_1/R_1$ and $Q_2 = \omega_0 L_2/R_2$ are the quality factors of the transmitter loop and receiver loop, respectively. η_{coil} is maximized when

$$\frac{U_1}{U_2} = \sqrt{\frac{R_1}{R_2}}. \tag{6}$$

B. Model With a CPL

For a given P_{out}, R_L in Fig. 2 can be expressed as

$$R_{\text{L}} = \frac{P_{\text{out}}}{I_2^2} = \frac{U_{\text{th}}}{I_2} - R_{\text{th}}. \tag{7}$$

Taking I_2 as a variable, (7) can be transformed into

$$R_{\text{th}} I_2^2 - U_{\text{th}} I_2 + P_{\text{out}} = 0. \tag{8}$$

Thus, I_2, I_1, and U_{bat} can be derived as

$$I_2 = \frac{U_{\text{th}} + \sqrt{U_{\text{th}}^2 - 4R_{\text{th}}P_{\text{out}}}}{2R_{\text{th}}} = \frac{U_1 + \sqrt{U_1^2 - 4R_1 P_{\text{out}}}}{2\omega_0 M} \tag{9}$$

$$I_1 = \frac{U_{\text{th}} - \sqrt{U_{\text{th}}^2 - 4R_{\text{th}}P_{\text{out}}}}{2\omega_0 M} = \frac{U_1 - \sqrt{U_1^2 - 4R_1 P_{\text{out}}}}{2R_1} \tag{10}$$

$$U_{\text{rec}} = \frac{\pi}{2\sqrt{2}}\frac{\omega_0 M}{2R_1}\left(U_1 - \sqrt{U_1^2 - 4R_1 P_{\text{out}}}\right). \tag{11}$$

η_{coil} can be calculated as

$$\eta_{\text{coil}} = \frac{P_{\text{out}}}{\left\{\begin{array}{l} P_{\text{out}} + \left(\frac{1}{2R_1} + \frac{R_2}{2(\omega_0 M)^2}\right)(U_1^2 - 2R_1 P_{\text{out}}) \\ -\left(\frac{1}{2R_1} - \frac{R_2}{2(\omega_0 M)^2}\right)U_1\sqrt{U_1^2 - 4R_1 P_{\text{out}}} \end{array}\right\}}. \tag{12}$$

By letting $\partial\eta_{\text{coil}}/\partial U_1 = 0$ in (12), the optimal U_1 to achieve the maximum η_{coil} at P_{out} is

$$U_{1-\text{opt}} = \sqrt{\left(\text{FOM} - \frac{1}{\text{FOM}} + 2\right) R_1 P_{\text{out}}}. \tag{13}$$

Replacing U_1 in (12) with (13) yields

$$\eta_{\text{coil-max}} = \frac{2}{\left\{\begin{array}{l} 2 + \left(1 + \frac{1}{\text{FOM}^2}\right)\left(\text{FOM} - \frac{1}{\text{FOM}}\right) \\ -\left(1 - \frac{1}{\text{FOM}^2}\right)\sqrt{\left(\text{FOM} - \frac{1}{\text{FOM}} + 2\right)\left(\text{FOM} - \frac{1}{\text{FOM}}\right)} \end{array}\right\}} \approx \frac{\text{FOM}}{\text{FOM} + 1}. \tag{14}$$

Similarly, the optimal I_1, I_2, and U_2 can be obtained. $\eta_{\text{coil}-\text{max}}$ increases monotonically with FOM.

When designing a WPT system with voltage tuning for the rated P_{out}, normally the coil geometry and the range of U_1 and U_2 are given. Thus, FOM can be estimated and U_1 and U_2 can be decided according to (6) and (13). The coils can be designed based on (3).

In this section, the SS topology is adopted for analysis. Different topologies have different expressions of U_{th} and R_{th}. The relationship between the transmitter-side quantities and the receiver-side quantities is also determined by the resonant topologies. Nevertheless, by adopting the TEC on the receiver side, the derivation aforementioned can be easily applied to other resonant topologies.

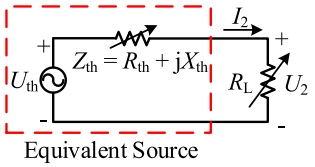

Fig. 3. TEC OFF resonance.

III. Frequency Tuning

For frequency tuning of a WPT system, the TEC on the receiver side is shown in Fig. 3, where Z_{th} is the Thevenin impedance and R_{th} and Z_{th} are the real part and the imaginary part of Z_{th}. U_{th} and Z_{th} can be expressed, respectively, as

$$U_{th} = \frac{\omega M U_1}{\sqrt{R_1^2 + X_1^2}} \tag{15}$$

$$Z_{th} = \left(R_2 + \frac{(\omega M)^2 R_1}{R_1^2 + X_1^2}\right) + j\left(X_2 - \frac{(\omega M)^2 X_1}{R_1^2 + X_1^2}\right) \tag{16}$$

where X_1 and X_2 are the transmitter and receiver reactances, expressed as $X_1 = \omega L_1 - 1/(\omega C_1)$ and $X_2 = \omega L_2 - 1/(\omega C_2)$.

Assume U_{th} leads U_2 for φ, which can be calculated by

$$I_2 = \frac{U_{th}\cos\varphi - U_2}{R_{th}} = \frac{U_{th}\sin\varphi}{X_{th}}. \tag{17}$$

Once φ is known, I_2 and all other parameters can be obtained accordingly. P_{out} at R_L can be expressed as

$$P_{out} = \frac{U_{th}^2 R_L}{(R_{th} + R_L)^2 + X_{th}^2}. \tag{18}$$

By letting $\partial P_{out}/\partial R_L = 0$ in (18), the maximum output power $P_{out-max}$ can be obtained as

$$P_{out\text{-}max} = \frac{U_{th}^2}{2\left(\sqrt{R_{th}^2 + X_{th}^2} + R_{th}\right)}. \tag{19}$$

When deviating from f_0, the changing rates of U_{th} and R_{th} are much smaller than that of X_{th}. Therefore, $P_{out-max}$ will peak at the zero point of X_{th}. There are three frequency points to satisfy $X_{th} = 0$: at, above, and below f_0, obtained as

$$X_{th} = X_2 - \frac{(\omega M)^2 X_1}{R_1^2 + X_1^2} = 0. \tag{20}$$

A. General Model With a CPL

At P_{out}, the model in Fig. 3 can be established by

$$\begin{cases} U_{th}^2 = \left[(R_{th} + R_L)^2 + X_{th}^2\right] I_2^2 \\ R_L = \dfrac{P_{out}}{I_2^2}. \end{cases} \tag{21}$$

Eliminating R_L in (21) yields

$$\left(R_{th}^2 + X_{th}^2\right) I_2^4 - \left(U_{th}^2 - 2R_{th}P_{out}\right) I_2^2 + P_{out}^2 = 0. \tag{22}$$

Considering I_2 in (22) as a variable, there are two real roots, indicating that there are two operation points for the target P_{out}. The corresponding two roots of I_2 can be derived as

$$I_2 = \sqrt{\frac{2P_{out}^2}{U_{th}^2 - 2R_{th}P_{out} \pm \sqrt{\left(U_{th}^2 - 2R_{th}P_{out}\right)^2 - 4P_{out}^2\left(R_{th}^2 + X_{th}^2\right)}}}. \tag{23}$$

When $P_{out} \le P_{out-max}$, the discriminant in (23) would satisfy

$$\Delta = \left(U_{th}^2 - 2R_{th}P_{out}\right)^2 - 4P_{out}^2\left(R_{th}^2 + X_{th}^2\right) \ge 0. \tag{24}$$

I_1, U_{rec}, and the system input impedance Z_{in} can be obtained, respectively, as

$$I_1 = \frac{1}{\omega M}\sqrt{\frac{P_{out}^2}{I_2^2} + X_2^2 I_2^2}, \quad U_{rec} = \frac{\pi}{2\sqrt{2}}\frac{P_{out}}{I_2} \tag{25}$$

$$Z_{in} = R_1 + jX_1 + \frac{(\omega M)^2}{R_1 + jX_2 + \frac{P_{out}}{I_2}}. \tag{26}$$

η_{coil} can be calculated as

$$\eta_{coil} = \frac{P_{out}}{P_{out} + \frac{R_1 P_{out}^2}{(\omega M)^2 I_2^2} + \left(\frac{X_2^2 R_1}{(\omega M)^2} + R_2\right) I_2^2}. \tag{27}$$

By letting $\partial\eta_{coil}/\partial I_2 = 0$, the optimal I_2 and U_{rec} to achieve $\eta_{coil-max}$ at P_{out} are

$$I_{2-opt} = \sqrt{\frac{P_{out}}{\sqrt{X_2^2 + \frac{R_2}{R_1}(\omega M)^2}}} \tag{28}$$

$$U_{rec-opt} = \frac{\pi}{2\sqrt{2}}\sqrt{P_{out}\sqrt{X_2^2 + \frac{R_2}{R_1}(\omega M)^2}}. \tag{29}$$

The optimal operating frequency can be calculated by letting I_2 in (23) equal the optimal value in (28). For a given U_1, the range for the operating frequency is limited, and the range can be calculated by the fact that discriminant shown in (24) should be no smaller than zero.

B. Simplified Model With a CPL

The model developed in Section III-A is complicated and may not offer an intuitive understanding of a WPT system with a CPL under frequency tuning. In this section, the model is simplified. Based on the maximum power transfer theorem of an ac circuit, the source available power in Fig. 3 is

$$P_{src\text{-}ava} = \frac{U_{th}^2}{4R_{th}}. \tag{30}$$

Note that $P_{src-ava}$ is achieved when the load impedance is the conjugate of Z_{th}. In a WPT system where a rectifier is employed to connect the receiver to the dc load, the rectifier can be regarded as purely resistive. Therefore, $P_{src-ava}$ cannot be achieved in such a condition.

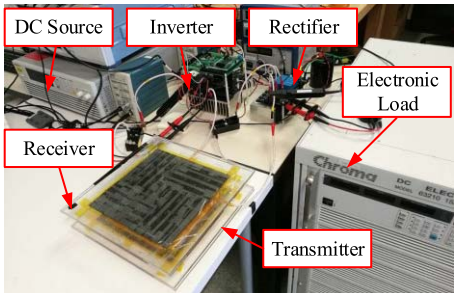

Fig. 4. Photograph of the experimental prototype.

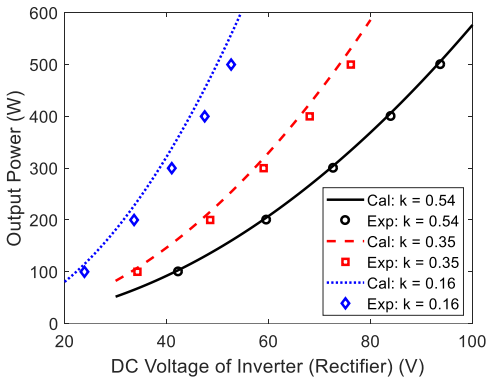

Fig. 5. P_{out} versus U_{inv} and U_{rec} via voltage tuning.

When $P_{\text{src-ava}} = U_{\text{th}}^2/(4R_{\text{th}}) \geq 10P_{\text{out}}$, we have $0.95U_{\text{th}}^2 \leq (U_{\text{th}}^2 - 2P_{\text{out}}R_{\text{th}}) \leq U_{\text{th}}^2$. Thus, $U_{\text{th}}^2 - 2P_{\text{out}}R_{\text{th}} \approx U_{\text{th}}^2$. Under this condition and ignoring X_{th}, the smaller root in (23) is

$$I_2 \approx \frac{P_{\text{out}}}{U_{\text{th}}}. \tag{31}$$

In this case, I_1 and U_{rec} can be expressed as

$$I_1 = \frac{1}{\omega M}\sqrt{U_{\text{th}}^2 + \frac{P_{\text{out}}^2}{U_{\text{th}}^2}X_2^2} \approx \frac{U_{\text{th}}}{\omega M}, \quad U_{\text{rec}} = \frac{\pi}{2\sqrt{2}}U_{\text{th}}. \tag{32}$$

η_{coil} can be obtained as

$$\eta_{\text{coil}} = \frac{P_{\text{out}}}{P_{\text{out}} + \frac{U_{\text{th}}^2}{(\omega M)^2}R_1 + \frac{P_{\text{out}}^2}{U_{\text{th}}^2}R_2} \tag{33}$$

which is maximized when

$$U_{\text{th-opt}} = \frac{\omega M U_1}{\sqrt{R_1^2 + X_1^2}} = \sqrt{\sqrt{\frac{R_2}{R_1}}\omega M P_{\text{out}}} \tag{34}$$

$$U_{\text{rec-opt}} = \frac{\pi}{2\sqrt{2}}\sqrt{\sqrt{\frac{R_2}{R_1}}\omega M P_{\text{out}}}. \tag{35}$$

The optimal operating frequency can be obtained by (34).

When designing a WPT system with frequency tuning for the rated P_{out}, normally the coil geometry, the operating frequency, and the range of U_1 and U_2 are given. Thus, U_{rec} and the coils can be determined according to (29).

Similar to Section II, in this section, the TEC of the SS topology is adopted and it can be easily applied to other topologies by changing the expressions of U_{th} and Z_{th} based on the topologies to be studied.

IV. Calculations and Experiments

An experimental prototype is implemented, depicted in Fig. 4. The transmitter and receiver coils are identical and have a size of 200 mm × 200 mm and a turn number of 12. The inner diameter is 95 mm. American wire gauge 38 Litz wires with 800 strands are employed. The size of the ferrite plate is 224 mm × 224 mm × 2 mm and $C_1 = C_2 = 77.5$ nF. At the charging distance of 38 mm, $k = 0.54$ and $L_1 = L_2 = 51.9$ μH; at 60 mm, $k = 0.35$ and $L_1 = L_2 = 48.6$ μH; and at 104 mm, $k = 0.16$ and $L_1 = L_2 = 47.1$ μH. Thus, the resonant frequencies are 79.4, 82.0, and 83.3 kHz. The measured quality factors of the coils increase by 10% from 80 to 150 kHz and can be assumed to be 480. A full-bridge inverter is utilized as the source with silicon carbide power MOSFET C2M0080120D as the switches. A full-bridge rectifier is employed as the load with fast recovery epitaxial diode DSEI120-06A as the switches. The ON-state resistance of the MOSFET is 100 mΩ and that of the diode is 3.5 mΩ. Given the switch ON-state resistances and the equivalent resistances of the capacitors, the quality factor of the transmitter loop is approximately 80 and that of the receiver loop is 300. The loss that is not considered in R_1 and R_2 is assumed to occupy 2.5% of the total power. Therefore, the dc–dc efficiency (η_{sys}) is the product of η_{coil} and 97.5%.

A. Voltage Tuning

With voltage tuning, the operating frequency equals f_0 and U_{inv} is regulated. Note that in practical applications, a dc–dc converter is needed for regulation. In the experimental setup, U_{inv} is regulated via a dc source. Thus, the efficiency of the dc–dc converter is not considered in voltage tuning. When $U_{\text{inv}} = U_{\text{rec}}$, the calculations based on (3) and the experimental results of P_{out} versus U_{inv} and U_{rec} are shown in Fig. 5. Under the same U_{inv} and U_{rec}, a smaller coupling leads to a larger P_{out}. The proposed model matches the experimental results well.

By regulating P_{out} to 500 W, the calculations based on (11) and (12) and the experimental results of U_{rec} and η_{sys} versus U_{inv} are given in Fig. 6. For a given P_{out}, U_{rec} decreases with the increasing U_{inv}. Even though the transmitter and receiver coils are identical, the equivalent resistance of the transmitter loop is larger than that of the receiver loop. Therefore, the efficiency peaks at a larger U_{inv} and a smaller U_{rec}, according to (6). Therefore, when designing a WPT system with the rated P_{out}, it is better with a larger U_{inv} and a smaller U_{rec} to achieve high efficiency and reduce the voltage rating of the rectifier. When $k = 0.16$, I_1 and I_2 to output 500 W are larger than those when $k = 0.54$ and 0.35. Thus, the efficiency of the power electronics converters for $k = 0.16$ is smaller than the other two coupling cases, leading to the gap between the calculations and the experimental results of η_{sys} when $k = 0.16$.

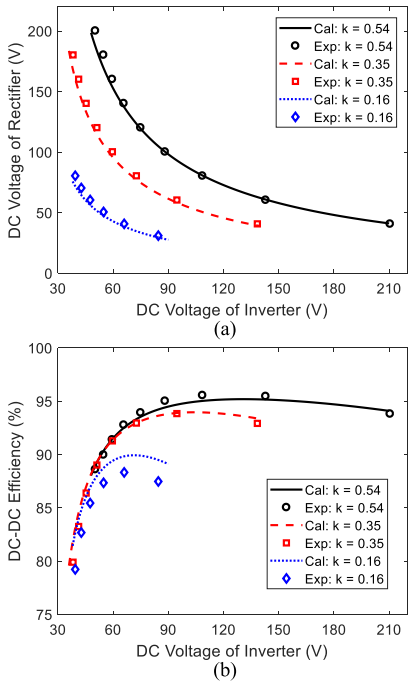

Fig. 6. (a) U_{rec} and (b) η_{sys} versus U_{inv} with a CPL via voltage tuning.

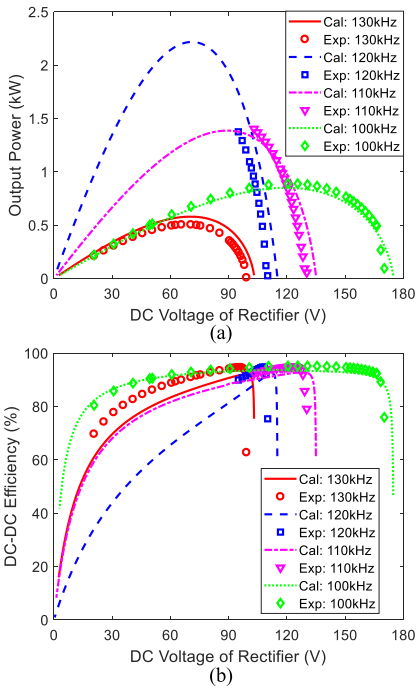

Fig. 8. (a) P_{out} and (b) η_{sys} versus U_{rec} under different frequencies when $U_{\text{inv}} = 120$ V and $k = 0.54$.

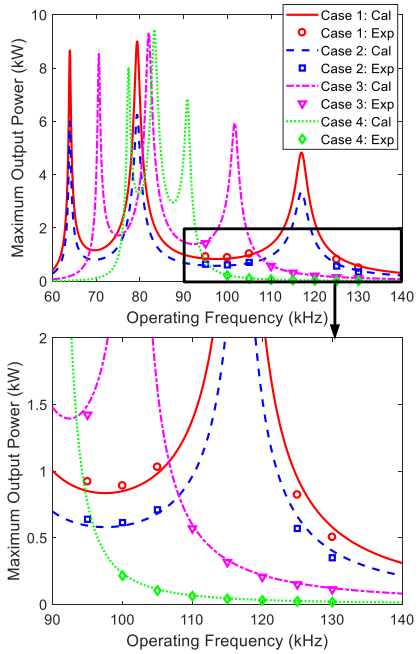

Fig. 7. $P_{\text{out-max}}$ versus the operating frequency.

B. Frequency Tuning

Four cases are studied for frequency tuning: case 1: $U_{\text{inv}} = 120$ V and $k = 0.54$, case 2: $U_{\text{inv}} = 100$ V and $k = 0.54$, case 3: $U_{\text{inv}} = 120$ V and $k = 0.35$, and case 4: $U_{\text{inv}} = 120$ V and $k = 0.16$.

The calculations, based on (19), and the experimental results of $P_{\text{out-max}}$ versus the operating frequency are shown in Fig. 7. There are three peaks for $P_{\text{out-max}}$, corresponding to the three zero points of X_{th} in (20). The resonant frequencies of case 1(2), case 3, and case 4 are different, leading to different frequency locations of the central peaks. U_{inv} affects the amplitude of P_{out} but has no impact on the location of these three peaks, while a smaller k results in smaller gaps between the peaks. Also, a strong coupling does not necessarily indicate a large $P_{\text{out-max}}$. There is a right tuning zone above f_0 and a left tuning zone below f_0. The former is much wider than the latter. The experimental results agree well with the calculations, despite the fact that not all calculations are validated due to the current constraint of the switches.

For case 1 when $U_{\text{inv}} = 120$ V and $k = 0.54$, the calculations based on (18) and (27) and the experimental results of P_{out} and η_{sys} versus U_{rec} under different frequencies are depicted in Fig. 8. There are two operating points of 500-W output in these four cases: a larger U_{rec} and a smaller U_{rec}, as indicated by (23). η_{sys} with a larger U_{rec} is higher than the other one because I_1 and I_2 are smaller, leading to a smaller loss. Therefore, in the following experiments for the rated P_{out}, only the point with a larger U_{rec} is selected. It can be seen from Fig. 8 that the peak P_{out} of 120 kHz is the highest among the four cases. This is in accordance with Fig. 7, where $P_{\text{out-max}}$ of case 1 peaks at round 118 kHz, which is when $X_{\text{th}} = 0$. Therefore, $P_{\text{out-max}}$ at 120 kHz is the highest, followed by 120, 110, and 130 kHz in sequence as indicated in Fig. 7.

With frequency tuning, P_{out} is tuned to 500 W. The amplitude and angle of Z_{in}, based on (26), of these four cases are shown in Fig. 9. The amplitude of Z_{in} in the proximity of the resonant frequency is very small, which means I_1 is very large, leading to a very low efficiency. The right tuning zone has an inductive Z_{in} and it is good for achieving high efficiency of the inverter by realizing zero-voltage switching (ZVS). Therefore, only the right tuning zone is considered.

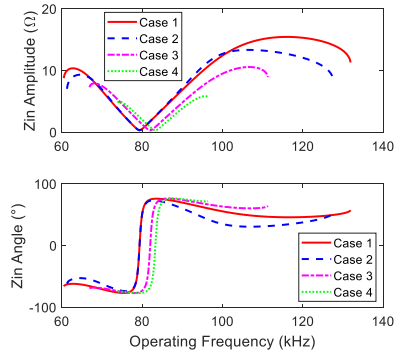

Fig. 9. Amplitude and angle of Z_{in} of four cases with a 500-W output.

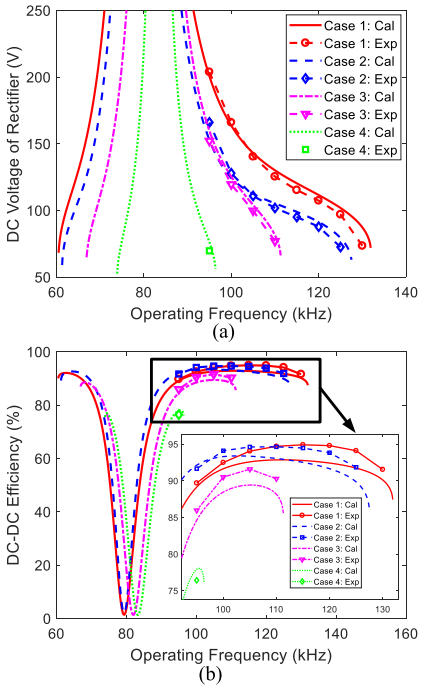

Fig. 10. (a) U_{rec} and (b) η_{sys} versus operating frequency with a CPL.

The calculations, based on (25), (27), and (29), and the experimental results of U_{rec}, η_{sys}, I_1, and I_2 versus the operating frequency under a CPL are plotted in Figs. 10 and 11. It can be seen that at the resonant frequency, U_{rec} is very high for the rated P_{out}. In the right tuning zone, U_{rec} decreases and I_2 increases with the operating frequency. There is a valley value of I_1, corresponding to the highest η_{sys}. Therefore, the system should operate at this point where η_{sys} is high and U_{rec} is low. This optimal point can be obtained from (30) and (31). Also, increasing U_{inv} and k extend the tuning range, but the former has a negligible impact on the maximum η_{sys} and the optimal U_{rec}, while the latter enhances them.

In addition, comparing Figs. 6 and 10, the maximum η_{sys} for voltage tuning when $k = 0.54$ is 95.56% and that when $k = 0.35$ is 93.84%. While for frequency tuning, the maximum η_{sys} when $k = 0.54$ is 94.92% and that when $k = 0.35$ is 91.59%. Larger k leads to the smaller gap between the maximum η_{sys} of voltage tuning and frequency tuning. With a larger k, η_{sys} of frequency tuning is slightly smaller than that

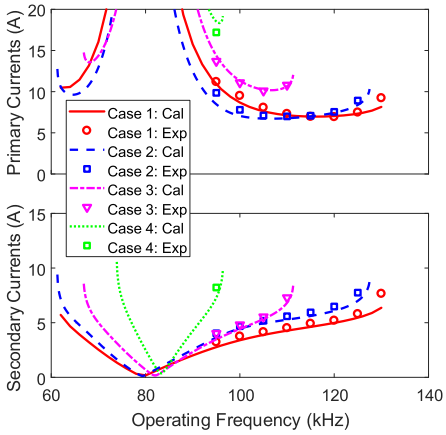

Fig. 11. I_1 and I_2 versus operating frequency with a CPL.

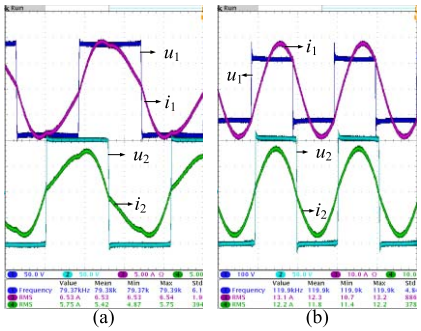

Fig. 12. Experimental waveforms when $k = 0.54$. (a) Voltage tuning at 79.4 kHz. (b) Frequency tuning at 120 kHz.

of voltage tuning, even though the efficiency is claimed to be maximized at the receiver resonant frequency [19]. When $k = 0.16$, the maximum η_{sys} of voltage tuning is 88.33% and that of frequency tuning is 76.42%, with a drop of more than 10%. Therefore, with a small k, frequency tuning is not suitable to achieve a high η_{sys}.

The experimental waveforms of voltage tuning and frequency tuning when $k = 0.54$ are depicted in Fig. 12. For voltage tuning, the WPT system works at f_0. Thus, Z_{in} is resistive and u_1 is in phase with i_1, which cannot achieve ZVS. In comparison, for frequency tuning, the WPT system works above f_0. Thus, Z_{in} is inductive and i_1 lags behind u_1, which helps to achieve ZVS.

V. Conclusion

For the design and optimization of a WPT system with a target output power, it is important to model a WPT system with a CPL and analyze its transfer characteristics so as to achieve high efficiency and restrict the rectifier dc voltage. In this paper, an SS compensated WPT system with a CPL under voltage tuning and frequency tuning has been modeled and analyzed. The closed-form expressions of the transmitter current, the receiver current, the rectifier dc voltage, and the coil-to-coil efficiency have been derived.

For voltage tuning, there is an optimal inverter dc voltage to achieve the maximum efficiency. When the equivalent

transmitter resistance is larger than the equivalent receiver resistance, the inverter dc voltage should be larger than that of the receiver to achieve high efficiency. For frequency tuning, the right tuning zone is selected because of its wide tuning range and achieving ZVS. The maximum output power at different operating frequencies has been obtained. Increasing the inverter dc voltage will extend the operating frequency range but will not impact the maximum efficiency and the optimal rectifier dc voltage. Increasing the coupling coefficient will also extend the operating frequency range, improve the efficiency, and increase the optimal rectifier dc voltage.

With a strong coupling (typically larger than 0.5), the maximum dc–dc efficiency of frequency tuning can be as high as that of voltage tuning. When the coupling coefficient is smaller than 0.2, the maximum dc–dc efficiency of frequency tuning is much smaller than that of voltage tuning.

REFERENCES

[1] C. C. Mi, G. Buja, S. Y. Choi, and C. T. Rim, "Modern advances in wireless power transfer systems for roadway powered electric vehicles," *IEEE Trans. Ind. Electron.*, vol. 63, no. 10, pp. 6533–6545, Oct. 2016.

[2] S. Li and C. C. Mi, "Wireless power transfer for electric vehicle applications," *IEEE J. Emerg. Sel. Topics Power Electron.*, vol. 3, no. 1, pp. 4–17, Mar. 2015.

[3] S. Y. R. Hui, W. Zhong, and C. K. Lee, "A critical review of recent progress in mid-range wireless power transfer," *IEEE Trans. Power Electron.*, vol. 29, no. 9, pp. 4500–4511, Sep. 2014.

[4] J. M. Miller, O. C. Onar, and M. Chinthavali, "Primary-side power flow control of wireless power transfer for electric vehicle charging," *IEEE J. Emerg. Sel. Topics Power Electron.*, vol. 3, no. 1, pp. 147–162, Mar. 2015.

[5] P. Si, A. P. Hu, S. Malpas, and D. Budgett, "A frequency control method for regulating wireless power to implantable devices," *IEEE Trans. Biomed. Circuits Syst.*, vol. 2, no. 1, pp. 22–29, Mar. 2008.

[6] R. Bosshard, U. Badstübner, J. W. Kolar, and I. Stevanović, "Comparative evaluation of control methods for inductive power transfer," in *Proc. Int. Conf. Renew. Energy Res. Appl. (ICRERA)*, Nov. 2012, pp. 1–6.

[7] D.-W. Seo and J.-H. Lee, "Frequency-tuning method using the reflection coefficient in a wireless power transfer system," *IEEE Microw. Wireless Compon. Lett.*, vol. 27, no. 11, pp. 959–961, Nov. 2017.

[8] H. Zeng, N. S. González-Santini, Y. Yu, S. Yang, and F. Z. Peng, "Harmonic burst control strategy for full-bridge series-resonant converter-based EV charging," *IEEE Trans. Power Electron.*, vol. 32, no. 5, pp. 4064–4073, May 2017.

[9] W. Zhong and S. Y. R. Hui, "Charging time control of wireless power transfer systems without using mutual coupling information and wireless communication system," *IEEE Trans. Ind. Electron.*, vol. 64, no. 1, pp. 228–235, Jan. 2017.

[10] H. Li, J. Li, K. Wang, W. Chen, and X. Yang, "A maximum efficiency point tracking control scheme for wireless power transfer systems using magnetic resonant coupling," *IEEE Trans. Power Electron.*, vol. 30, no. 7, pp. 3998–4008, Jul. 2015.

[11] A. Berger, M. Agostinelli, S. Vesti, J. A. Oliver, J. A. Cobos, and M. Huemer, "A wireless charging system applying phase-shift and amplitude control to maximize efficiency and extractable power," *IEEE Trans. Power Electron.*, vol. 30, no. 11, pp. 6338–6348, Nov. 2015.

[12] Y. Zhang, T. Lu, Z. Zhao, F. He, K. Chen, and L. Yuan, "Employing load coils for multiple loads of resonant wireless power transfer," *IEEE Trans. Power Electron.*, vol. 30, no. 11, pp. 6174–6181, Nov. 2015.

[13] T. Kan, T.-D. Nguyen, J. C. White, R. K. Malhan, and C. C. Mi, "A new integration method for an electric vehicle wireless charging system using LCC compensation topology: Analysis and design," *IEEE Trans. Power Electron.*, vol. 32, no. 2, pp. 1638–1650, Feb. 2017.

[14] S. Y. Choi, J. Huh, W. Y. Lee, and C. T. Rim, "Asymmetric coil sets for wireless stationary EV chargers with large lateral tolerance by dominant field analysis," *IEEE Trans. Power Electron.*, vol. 29, no. 12, pp. 6406–6420, Dec. 2014.

[15] X. Dai, X. Li, Y. Li, and A. P. Hu, "Impedance-matching range extension method for maximum power transfer tracking in IPT system," *IEEE Trans. Power Electron.*, vol. 33, no. 5, pp. 4419–4428, May 2018.

[16] Y. Zhang, K. Chen, F. He, Z. Zhao, T. Lu, and L. Yuan, "Closed-form oriented modeling and analysis of wireless power transfer system with constant-voltage source and load," *IEEE Trans. Power Electron.*, vol. 31, no. 5, pp. 3472–3481, May 2015.

[17] U. K. Madawala and D. J. Thrimawithana, "A bidirectional inductive power interface for electric vehicles in V2G systems," *IEEE Trans. Ind. Electron.*, vol. 58, no. 10, pp. 4789–4796, Oct. 2011.

[18] C. Zhao, Z. Wang, J. Du, J. Wu, S. Zong, and X. He, "Active resonance wireless power transfer system using phase shift control strategy," in *Proc. Annu. IEEE Appl. Power Electron. Conf. Expo. (APEC)*, Mar. 2014, pp. 1336–1341.

[19] Y. Zhang, Z. Zhao, and K. Chen, "Frequency decrease analysis of resonant wireless power transfer," *IEEE Trans. Power Electron.*, vol. 29, no. 3, pp. 1058–1063, Mar. 2014.

Yiming Zhang (S'13–M'16) received the B.S. and Ph.D. degrees in electrical engineering from Tsinghua University, Beijing, China, in 2011 and 2016, respectively.

He is currently a Post-Doctoral Researcher with San Diego State University, San Diego, CA, USA. His current research interests include wireless power transfer for electric vehicles and mobile phones and resonant converters.

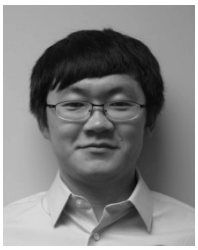

Tianze Kan (S'15) received the B.Eng. degree in electrical engineering and automation from the Huazhong University of Science and Technology, Wuhan, China, in 2011, and the M.S. degree in electrical engineering from the University of Southern California, Los Angeles, CA, USA, in 2013. He is currently pursuing the Ph.D. degree in electrical and computer engineering in the joint doctoral program between San Diego State University, San Diego, CA, USA, and the University of California San Diego, La Jolla, CA, USA.

His current research interests include power electronics and inductive-based wireless power transfer, especially on coil design and compensation topologies.

Zhengchao Yan (S'18) received the B.S. degree in mechanical design, manufacturing, and automation from Northwestern Polytechnical University, Xi'an, China, in 2013, where he is currently pursuing the Ph.D. degree.

In 2017, he received the funding from China Scholarship Council, and became a joint Ph.D. student with the Department of Electrical and Computer Engineering, San Diego State University, San Diego, CA, USA.

His current research interests include wireless power transfer, including coil design and compensation topologies.

Chunting Chris Mi (S'00–A'01–M'01–SM'03–F'12) received the B.S.E.E. and M.S.E.E. degrees in electrical engineering from Northwestern Polytechnical University, Xi'an, China, in 1985 and 1988, respectively, and the Ph.D. degree in electrical engineering from the University of Toronto, Toronto, ON, Canada, in 2001.

From 2001 to 2015, he was with the University of Michigan, Dearborn, MI, USA. He is currently a Professor and the Chair of electrical and computer engineering and the Director of the Department of Energy, funded Graduate Automotive Technology Education Center for Electric Drive Transportation, San Diego State University, San Diego, CA, USA. His current research interests include electric drives, power electronics, electric machines, renewable-energy systems, and electric and hybrid vehicles.